

# Comparison of the spatial and the angular clustering of X-ray AGN

L. Koutoulidis<sup>1,2</sup> M. Plionis<sup>3,1,4</sup> and I. Georgantopoulos<sup>1</sup> A. Georgakakis<sup>5,1</sup> A. Akylas<sup>1</sup> S. Basilakos<sup>6</sup> G. Mountrichas<sup>1</sup>

<sup>1</sup> IAASARS, National Observatory of Athens, I. Metaxa & V. Pavlou 1, Penteli, 15236, Greece

<sup>2</sup> Astronomical Laboratory, Department of Physics, University of Patras, 26500 Rio-Patras, Greece

<sup>3</sup> Physics Department, University of Thessaloniki, Thessaloniki 54124, Greece

<sup>4</sup> Instituto Nacional de Astrofísica, Óptica y Electrónica, Luis Enrique Erro 1, Tonantzilla, Puebla, México

<sup>5</sup> Max-Planck-Institut für Extraterrestrische Physik (MPE), Postfach 1312, 85741, Garching, Germany

<sup>6</sup> Academy of Athens, Research Center for Astronomy and Applied Mathematics, Soranou Efessiou 4, 11527, Athens, Greece

## ABSTRACT

The angular correlation function is a powerful tool for deriving the clustering properties of AGN and hence the mass of the corresponding dark matter halos in which they reside. However, recent studies based on the application of the angular correlation function on X-ray samples, yield results apparently inconsistent with those based on the direct estimation of the spatial correlation function. The goal of the present paper is to attempt to investigate this issue by analysing a well defined sample. To this end we use the hard-band (2–10 keV) X-ray selected sources of the Chandra AEGIS fields, chosen because of the availability of accurately derived flux sensitivity maps. In particular we use the 186 hard-band sources with spectroscopic redshifts in the range  $z = 0.3–1.3$ , a range selected in order to contain the bulk of the AGN while minimizing the contribution of unknown clustering and luminosity evolution from very high redshifts. Using the projected spatial auto-correlation function, we derive a clustering comoving length of  $x_0 = 5.4 \pm 1.0 h^{-1}$  Mpc (for  $\gamma = 1.8$ ), consistent with results in the literature. We further derive the angular correlation function and the corresponding spatial clustering length using the Limber’s inversion equation and a novel parametrization of the clustering evolution model that also takes into account the bias evolution of the host dark matter halo. The Limber’s inverted spatial comoving clustering length of  $x_0 = 5.5 \pm 1.2 h^{-1}$  Mpc at a median redshift of  $z \simeq 0.75$ , matches the directly measured one, from the spatial correlation function analysis, but for a significant non-linear contribution to the growing mode of perturbations, estimated independently from literature results of  $x_0$  at different redshifts. Therefore, using this sample of hard X-ray AGN and our clustering evolution parametrization we have found an excellent consistency between the angular and spatial clustering analysis.

**Key words.** active galaxies – clustering – X-rays – galaxies

## 1. Introduction

The triggering mechanism for the AGN activity is still an open issue (Alexander & Hickox 2012). Several semi-analytical models which include major galaxy mergers can explain the triggering mechanism for the most luminous AGN (Di Matteo et al. 2005; Hopkins et al. 2006) while it is possible that in the lowest luminosity AGN regime secular evolution (disk instabilities or minor interactions) may play the key role (Hopkins & Hernquist 2006; Bournaud et al. 2011).

Measuring the clustering of AGN can place valuable constraints on the AGN fueling modes and also provide us important information for the AGN activity and their dark matter halo hosts. Merger models appear to reproduce the clustering of QSOs and the mass of dark matter halo in which they reside. However in the X-ray regime, clustering of X-ray AGN shows evidence that they live in more massive dark matter halos, one order of magnitude larger (Koutoulidis et al. 2013) than the optical QSOs. This result suggest that the main accretion mode is the so-called hot halo mode (Fanidakis et al. 2012, 2013).

The clustering of AGN has been studied with excellent number statistics in the optical bands, particularly in large area surveys such as the 2QZ (Croom et al. 2005; Porciani & Norberg

2006) and the SDSS (Sloan Digital Sky Survey) (Li et al. 2006; Shen et al. 2009; Ross et al. 2009). However, optical QSO may represent only the tip of the iceberg of the AGN population. X-ray surveys find a surface density of about  $20,000 \text{ deg}^{-2}$  (Xue et al. 2011) which is about two orders of magnitude higher than that found in optical QSO surveys (Wolf et al. 2003). X-ray selected, spectroscopically identified AGN, form a superset of the optical selected AGN population since a large fraction of hard X-ray selected AGNs do not show strong optical activity (Barger 2005). Therefore, in order to study the clustering of the total AGN population we need X-ray samples. Recently, several studies have attempted to measure the spatial correlation function of X-ray selected AGN, using spectroscopic redshifts to estimate their distances at moderate redshifts (Mullis et al. 2004; Gilli et al. 2005; Yang et al. 2006; Gilli et al. 2009; Hickox et al. 2009; Coil et al. 2009; Krumpel et al. 2010; Starikova et al. 2011; Allevato et al. 2011; Koutoulidis et al. 2013) and at low redshifts (Cappelluti et al. 2010). Better statistics can be achieved using a cross correlation analysis with galaxies, either using spectroscopic AGN and galaxy samples (Coil et al. 2009; Krumpel et al. 2010; Mountrichas & Georgakakis 2012) or only spectroscopy for the AGNs and photometric redshifts (their pdfs) for the galaxies (Mountrichas et al. 2013). In order to derive directly

the spatial clustering length for a large sample of X-ray AGN an extensive spectroscopic campaign is required or high quality of photometric redshift measurements. However, even better statistics can be provided by the angular correlation function (ACF) for which all the detected sources are used, independently of the availability of spectroscopy.

Several studies have explored the angular clustering of AGN in X-ray wavelengths using data from *ROSAT* (Vikhlinin & Forman 1995; Akylas et al. 2000), from *XMM-Newton* (Basilakos et al. 2004, 2005; Puccetti et al. 2006; Ebrero et al. 2009; Miyaji et al. 2007; Elyiv et al. 2012) or deep pencil CDFs fields (Gilli et al. 2005; Plionis et al. 2008). These studies measure the projected angular clustering and then via Limber's equation (Peebles 1980) derive the corresponding spatial clustering length. Their results however appear to contradict the direct measurements of spatial clustering, with all the angular correlation analyses finding systematically larger correlation amplitudes. Possible reasons for this discrepancy include uncertainties in the X-ray AGN luminosity function and thus in the corresponding redshift distribution as well as the clustering evolution model, both of which are necessary for the Limber's inversion.

A way to break this impasse is to derive both the angular and spatial clustering for the same set of objects and compare directly their results. In this paper we derive the spatial correlation function in the AEGIS field in the hard band, using 186 sources with spectroscopic redshift information. Then we derive the angular correlation function (ACF) for exactly the same sources, to infer the spatial correlation length, using in one case the redshift distribution providing from luminosity function and in the other case the redshift distribution as it observed from the sources with spectroscopic redshifts.

The paper is organised as follows. In section 2 we present the AEGIS data, in section 3 we present our methodology and our modeling of the clustering evolution, while the results from our spatial and angular correlation function analysis, the Limber's inversion of the latter and the comparison of the two clustering lengths are presented in section 4. Throughout this work we adopt a flat  $\Lambda$ CDM cosmological model with  $H_0 = 100 \text{ km s}^{-1} \text{ Mpc}^{-1}$ .

## 2. AEGIS CATALOG

The ultra deep field survey comprises of pointings at 8 separate positions, each with a nominal exposure 200 ksec, covering a total area of approximately  $0.67 \text{ deg}^2$  and centered at  $a = 14^h 17^m$ ,  $\delta = +52^\circ 30'$  in a strip of length 2 degrees with a flux limit of  $3.8 \times 10^{-16} \text{ erg s}^{-1} \text{ cm}^{-2}$  in the hard band. We use X-ray source catalogue of Laird et al. (2009). In the hard band we have a total of 741 X-ray sources. Spectroscopic redshifts are available from the DEEP2 survey (Davis et al. 2001, 2003; Coil et al. 2009) for 312 sources spanning the  $0 < z < 4.3$  range. However, in the current work we will restrict our analysis to within the redshift interval  $z = 0.3 - 1.3$ , comprising 186 sources, in order to minimize strong evolutionary effects of the spatial correlation function and of the hard-band X-ray luminosity function, while having enough sources to obtain a relatively robust clustering signal. The median redshift of this spectroscopic subsample is  $\bar{z} = 0.75$ .

The advantage of using the AEGIS field for the purpose of this study is that source detection and sensitivity maps are constructed self-consistently following the method described in detail in Laird et al. (2009); Georgakakis et al. (2008), which is an analytical method that accurately estimates the probability of

detecting a source with a given X-ray flux at a given position on the detector accounting for vignetting and flux biases. Such sensitivity maps are essential for the production of accurate random catalogues and therefore for the reliable determination of the angular correlation function. It is likely that inconsistencies between the spatial and angular correlation function could, at least partially, originate from using sensitivity maps which are not consistent with the provided X-ray source lists.

## 3. METHODOLOGY

In order to quantify the low-order clustering of a distribution of sources, one uses the two-point correlation function which describes the excess probability over random of finding pairs of sources within a range of separations.

Depending on the availability or not of redshifts, one can use the spatial or angular correlation function. The former,  $\xi(r)$  involves sources within elemental volumes  $dV_i$  separated by a distance  $r$  (e.g., Peebles 1980), and is given by:  $dP = \langle n \rangle^2 [1 + \xi(r)] dV_1 dV_2$ , where  $\langle n \rangle$  is the mean space source density.

If redshifts are not available, one can measure the angular correlation function,  $w(\theta)$ , on the plane of sky which involves finding pairs of sources within infinitesimal solid angles,  $d\omega_i$ , separated by an angle  $\theta$ . The equivalent mathematical description is given by  $dP = \langle n \rangle^2 [1 + w(\theta)] d\omega_1 d\omega_2$ . On small scales  $w(\theta)$  has also been found to follow a power law behaviour:  $w(\theta) = (\theta/\theta_0)^\beta$  with  $\beta \simeq 1 - \gamma$ .

The actual correlation function estimator used, being either spatial or angular (generically indicated with  $\mathcal{W}$ ), is given by the expression (Hamilton 1993)

$$\mathcal{W} = \mathcal{N} \frac{DD \times RR}{DR^2} - 1 \quad (1)$$

with  $DD$ ,  $RR$  and  $DR$  the data-data, random-random, data-random pairs, respectively, at some separation  $r$  or  $\theta$ , while  $\mathcal{N}$  is a small correction equal to the ratio  $(N_D N_R)^2 / N_D (N_D - 1) N_R (N_R - 1)$  where  $N_D$  and  $N_R$  are the numbers of real and random data, respectively.

The variance of the correlation function at each separation is estimated according to:

$$\sigma_{\mathcal{W}}^2 = 3 \frac{(1 + \mathcal{W})^2}{DD}, \quad (2)$$

which corresponds to that expected by the bootstrap resampling technique (Mo et al. 1992). In order to estimate from the derived correlation function the values of the correlation length ( $r_0$  or  $\theta_0$ ) and of the slope  $\gamma$ , we use a  $\chi^2$  minimization procedure between the derived  $\mathcal{W}$  and the power law model:

$$\chi^2(r_0, \gamma) = \sum_{i=1}^n \frac{(\mathcal{W}_{data} - \mathcal{W}_{model})^2}{\sigma_{\mathcal{W}}^2} \quad (3)$$

where  $n$  is the number of separation bins. The minimization is over scales where the power-law appears to be a reasonable fit to the data (thus, very large and very small scales are excluded from the fit, which in our case translate to:  $r_p \lesssim 1$  and  $r_p \gtrsim 20 \text{ h}^{-1} \text{ Mpc}$ ).

### 3.1. Modelling the 2-point correlation function

The spatial correlation function of all different mass tracers of the large-scale structure of the Universe, being galaxies, AGN or clusters of galaxies, is described well by a power-law with two

free parameters,  $r_0$  and  $\gamma$ , the former related to the amplitude of clustering and the latter on the slope of the power-law. Locally, at  $z \simeq 0$ , it takes the form:

$$\xi(r) = \left(\frac{r}{r_0}\right)^{-\gamma} \quad (4)$$

where  $r$  is the proper separation between any two tracers. It has been found that  $\gamma \simeq 1.8$  for a wide range of mass tracers. In an evolving Universe the spatial correlation function is a function of redshift, as expected from the fact that the density perturbations evolve with redshift.

Traditionally the evolution of clustering has been parametrized with the use of the  $\epsilon$  parameter, proposed originally within the framework of the EdS model (Groth & Peebles 1977; Peebles 1980; de Zotti et al. 1990), which characterizes the different clustering evolution models according to:

$$\xi(r, z) = (1 + z)^{-(3+\epsilon)} \xi(r, 0) \quad (5)$$

Evidently, the value  $\epsilon = -3$  for which  $\xi(r, z) = \xi(r, 0)$  corresponds to constant clustering in proper coordinates, the value  $\epsilon = 0$  corresponds to the stable clustering scenario in which clusters remain bound and stable while due to the expansion the background density drops by  $(1 + z)^3$ , the value  $\epsilon = -1$  corresponds to the linear evolution (within the EdS model and neglecting the evolution of bias), while for  $\epsilon = \gamma - 3$  the clustering is constant in comoving coordinates, as it can be appreciated from the evolution of the correlation length given, for the case of a power law (eq.4), by:

$$r_0^\gamma(z) = \left(\frac{x_0}{1 + z}\right)^\gamma = r_0^\gamma (1 + z)^{-(3+\epsilon)} \quad (6)$$

and thus

$$x_0 = r_0 (1 + z)^{-(3+\epsilon-\gamma)/\gamma} \quad (7)$$

where  $x_0$  is the comoving correlation length at redshift  $z$  (and  $r_0 = x_0(0)$ ). We can now see that indeed if  $\epsilon = \gamma - 3$  we have a constant correlation length in comoving coordinates.

In this work we prefer to use a more physical modelling that takes into account both the cosmological evolution of perturbations and of the linear bias of the mass tracers. We start from the definition of the correlation function, given by:

$$\xi(r, z) = \langle \delta(\mathbf{x}, z) \delta(\mathbf{x} + \mathbf{r}, z) \rangle = b^2(z) \langle \delta_m(\mathbf{x}, z) \delta_m(\mathbf{x} + \mathbf{r}, z) \rangle \quad (8)$$

where  $\delta$  and  $\delta_m$  are the linear density contrasts for the tracers (in our case X-ray AGNs) and for the underlying Dark Matter (DM), respectively, and  $b(z)$  is the evolution of the linear bias factor. Therefore, since  $\delta_m$  evolves in the linear regime according to:

$$\delta_m(r, z) = \frac{D(z)}{D(0)} \delta_m(r, 0) \quad (9)$$

with  $D(z)$  the linear growing mode of the density perturbations, we have that:

$$\xi(r, z) = \frac{D^2(z)}{D^2(0)} b^2(z) \xi_m(r, 0) = \frac{D^2(z)}{D^2(0)} \frac{b^2(z)}{b^2(0)} \xi(r, 0), \quad (10)$$

with  $\xi(r, 0)$  the present epoch spatial correlation function of the X-ray AGN. Introducing the normalised to the present linear growing mode and bias as  $\tilde{D}(z) = D(z)/D(0)$  and  $\tilde{b}(z) = b(z)/b(0)$ , respectively, we write Eq.(10) as:  $\xi(r, z) = \tilde{D}^2(z) \tilde{b}^2(z) \xi(r, 0)$ . Note however that scales of a few Mpc, ie.,

around the clustering length of the spatial correlation function, should be affected by non-linear effects and therefore modelling its evolution only by the linear factor  $\tilde{D}^2(z)$  factor is inadequate. We therefore introduce a further factor  $\tilde{D}^n(z)$  where the exponent  $n$  absorbs the non-linear effects. Therefore, Eq.(10) becomes:

$$\xi(r, z) = \tilde{D}^{2+n}(z) \tilde{b}^2(z) \xi(r, 0), \quad (11)$$

and for a power law correlation function we obtain the evolution of the correlation length in proper coordinates,  $r_0(z)$ , as:

$$r_0^\gamma(z) = \left(\frac{x_0}{1 + z}\right)^\gamma = r_0^\gamma \tilde{D}^{2+n}(z) \tilde{b}^2(z) \quad (12)$$

which translates in comoving coordinates to:

$$x_0 = r_0 (1 + z) \tilde{D}^{(2+n)/\gamma}(z) \tilde{b}^{2/\gamma}(z). \quad (13)$$

It is important to appreciate the correspondence of the two different parametrizations of the clustering evolution. Comparing the generic formulation of eq.(11) with that of the  $\epsilon$  parametrization (eq. 5) we see that what is implied is the equivalence of  $\tilde{D}^{2+n}(z) \tilde{b}^2(z)$  with  $(1 + z)^{-(3+\epsilon)}$ , which however is valid only for as long as both  $\tilde{D}(z)$  (as for example in the EdS model) and  $\tilde{b}(z)$  (as for example in the usual galaxy conserving bias model (Fry 1996)) are power law functions of  $1 + z$ . However, in the general case of other than the EdS cosmological models and of a more general bias evolution model, valid also at large redshifts, (e.g., Sheth & Tormen 1999; Tinker et al. 2010; Basilakos et al. 2008), the above inferred equivalence and thus the  $\epsilon$  parametrization are not valid. For example, for the  $\Lambda$ CDM model the growing mode for the evolution of linear perturbations is given by (e.g., Peebles 1993):

$$D(z) = \frac{5\Omega_{m,0}E(z)}{2} \int_z^\infty \frac{(1+y)}{E^3(y)} dy \quad (14)$$

where  $E(z) = [\Omega_{m,0}(1 + z)^3 + \Omega_\Lambda]^{1/2}$  (for a flat  $\Lambda \neq 0$  model), while  $\Omega_{m,0}(z)$  and  $\Omega_\Lambda(z)$  are respectively the parametrized matter and cosmological constant density parameters. An EdS look-alike (normalised) fitting function of eq.(14) is:

$$\tilde{D}(z) = \frac{g(z)}{g(0)} \frac{1}{1 + z} = \frac{g(z)}{g(0)} \tilde{D}_{EdS}(z) \quad (15)$$

where  $g(z)$  is a function of  $\Omega_{m,0}(z)$  and  $\Omega_\Lambda(z)$  (Carroll, Press & Turner 1992; Lahav & Suto 2003).

It will be instructive to graphically compare the two parametrizations and appreciate their differences. To this end we use the bias evolution scheme of Basilakos & Plionis (2001, 2003) which is based on linear perturbation theory and given by (Basilakos et al. 2011):

$$b(z) = 1 + \frac{b_0 - 1}{D(z)} + C_2 \frac{J(z)}{D(z)} \quad (16)$$

with

$$J(z) = \int_0^z \frac{(1+y)}{E(y)} dy. \quad (17)$$

The constants  $b_0$  (the present day bias factor) and  $C_2$  depend on the host dark matter halo mass and for the  $\Lambda$ CDM model are given by:

$$b_0(M_h) = 0.857 \left[ 1 + \left( C_m \frac{M_h}{10^{14} h^{-1} M_\odot} \right)^{0.55} \right] \quad (18)$$

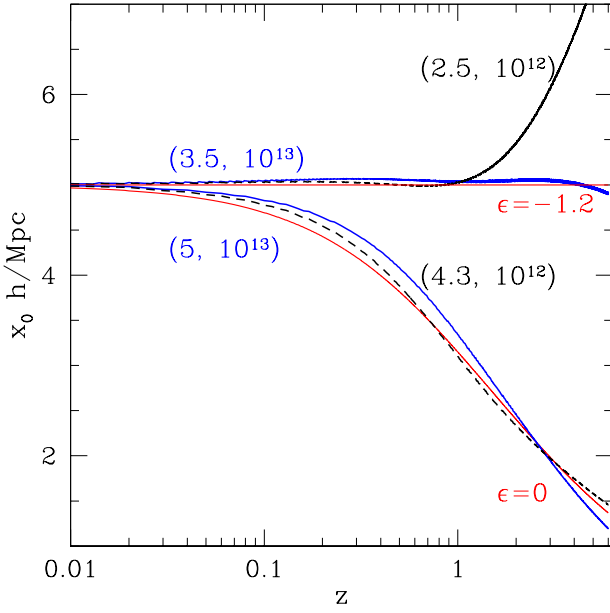


**Fig. 1.** The redshift evolution of the comoving clustering length for the two different parametrizations of the clustering evolution. For the case of our model (eq.13), shown as black and blue curves, the different evolution behaviors shown correspond to the indicated parameters  $(n, M_h)$ . The specific values of these parameters have been chosen such as to resemble the  $\epsilon = -1.2$  and  $\epsilon = 0$  models of the traditional parametrization of eq.(7), shown in red, which correspond to the constant in comoving coordinates clustering (for  $\gamma = 1.8$ ) and to the stable clustering models (for details see the text).

$$C_2(M_h) = 1.105 \left[ 1 + \left( C_m \frac{M_h}{10^{14} h^{-1} M_\odot} \right)^{0.255} \right] \quad (19)$$

where  $C_m = \Omega_{m,0}/0.27$  (Basilakos et al. 2012). This bias evolution model has been thoroughly tested and found to rate very well in reproducing N-body simulation data (Basilakos et al. 2008) as well as fitting observational data (Papageorgiou et al. 2012).

We therefore see that through the dependence of the bias factor on the dark matter halo mass one expects for the same values of  $n$  and  $\gamma$  a different clustering evolution for dark matter halos of different mass. In order to appreciate our parametrization of the clustering evolution we present in Figure 1 the evolution of the comoving clustering length  $x_0$  for models which have been on purpose selected to resemble some  $\epsilon$  based models. As can be seen the model with  $(n, M_h) = (3.5, 10^{13} M_\odot)$  is equivalent with the constant in comoving coordinates clustering model ( $\epsilon = \gamma - 3 = -1.2$ ) up to very large redshifts ( $z \sim 6$ ). No other  $(n, M_h)$  combination can provide such an equivalence up to such high redshifts. However, as we can again see in Fig.1 one can find  $(n, M_h)$  combinations that correspond to the comoving clustering model but up to  $z \simeq 1.2$ , as the example shown with  $(n, M_h) = (2.5, 10^{12} M_\odot)$ . In fact one can derive the degeneracy between the  $n$  and  $M_h$  parameters such that the clustering evolution is constant in comoving coordinates ( $\epsilon = -1.2$ ), but up to  $z \sim 1.2$ , since beyond this redshift the equivalence is unattainable. In Figure 2 we present the corresponding 1, 2 and 3  $\sigma$  contours in the  $(n, M_h)$  parameter space of the solution which provides the above equivalence with the  $\epsilon = -1.2$  model. The range is dictated by the uncertainty which we have imposed

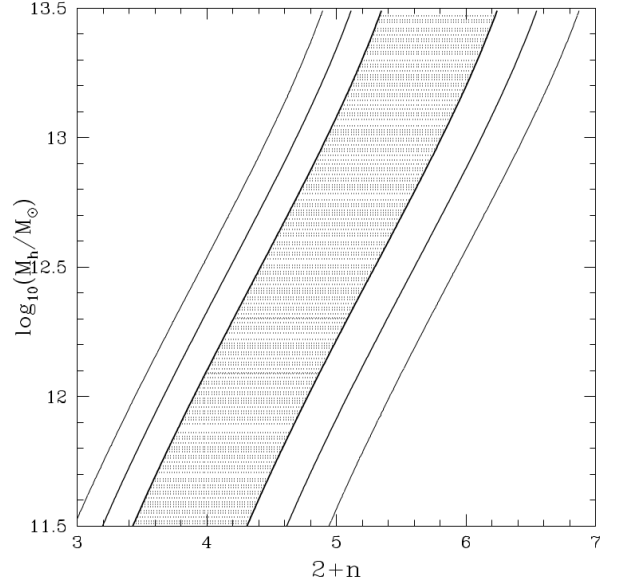


**Fig. 2.** The 1, 2 and 3  $\sigma$  contour range in the  $n, M_h$  parameter plane for the case where our clustering evolution scheme corresponds to the constant in comoving coordinates model (imposed up to  $z = 1$  in this example). The strong degeneracy of the parameters is evident.

on  $x_0$ , which is taken to be 10% of  $x_0$ , typical of current accurate measurements. The degeneracy is clear and it can only be broken if we either impose a value of  $n$ , for example from the expected slope of the power spectrum on these scales, or from an independent estimate of the mass of the dark matter halos in which the tracers (in our case X-ray selected AGN) reside.

Similarly, larger values of  $n$  provide clustering evolution behaviours that start resembling the  $\epsilon = 0$  stable clustering model. For example, we show in Fig.1 the  $(n, M_h) = (5, 10^{13} M_\odot)$  and the  $(4.3, 10^{12} M_\odot)$  which closely follow the  $\epsilon = 0$  model, indicating again the degeneracy problem discussed previously.

In what follows we will use a value for the dark matter halo mass derived from our previous spatial clustering analysis of Chandra X-ray selected AGN (Koutoulidis et al. 2013), i.e.,  $M_h \simeq 1.3 \times 10^{13} h^{-1} M_\odot$ . As we already saw, for this value of the halo mass and for  $n \simeq 5.5$  one obtains the constant in comoving coordinates model for the evolution of clustering.

### 3.2. Estimating the Spatial Correlation Function

Although the recessional velocities of extragalactic sources are used as distance indicators, they are contaminated by local peculiar velocities and thus the corresponding distances are distorted by the so-called redshift-space distortion effect. An estimator that avoids such effects, while using redshifts to infer distances, is the projected correlation function  $w_p(r_p)$  (Davis & Peebles 1983), which is based on deconvolving the redshift-based comoving distance,  $s$ , in a component parallel and perpendicular to the line of sight,  $\pi$  and  $r_p$ , respectively, i.e.,  $s^2 = r_p^2 + \pi^2$ . The redshift-space correlation function can therefore be written as:

$$\xi(s) = \xi(r_p, \pi) = \xi \left( \sqrt{r_p^2 + \pi^2} \right), \quad (20)$$

and the so-called projected correlation function can be found by integrating  $\xi(r_p, \pi)$  along the  $\pi$  direction:

$$w_p(r_p) = 2 \int_0^\infty \xi(r_p, \pi) d\pi. \quad (21)$$

Then the real space correlation function can be recovered according to (Davis & Peebles 1983):

$$w_p(r_p) = 2 \int_0^{\pi_{\max}} \xi\left(\sqrt{r_p^2 + \pi^2}\right) d\pi = 2 \int_{r_p}^\infty \frac{x \xi(x) dx}{\sqrt{x^2 - r_p^2}}. \quad (22)$$

Modelling  $\xi(x)$  as a power law one obtains:

$$w_p(r_p) = H_\gamma r_p \left(\frac{x_0}{r_p}\right)^\gamma \quad (23)$$

with  $x_0$  the comoving clustering length at the effective (median) redshift of the sample, and

$$H_\gamma = \Gamma\left(\frac{1}{2}\right) \Gamma\left(\frac{\gamma-1}{2}\right) / \Gamma\left(\frac{\gamma}{2}\right) \quad (24)$$

with  $\Gamma$  the usual gamma function. Note that eq.(22) holds strictly for  $\pi_{\max} = \infty$ , while in order to avoid redshift-space distortions the integral is performed up to a finite value of  $\pi_{\max}$ , which in turn produces an underestimation of the underlying correlation function. For a power law correlation function this underestimation is easily inferred from Eq.(22) and is given by (e.g., Starikova et al. 2011):

$$C_\gamma(r_p) = \frac{\int_0^{\pi_{\max}} (r_p^2 + \pi^2)^{-\gamma/2} d\pi}{\int_0^\infty (r_p^2 + \pi^2)^{-\gamma/2} d\pi}. \quad (25)$$

The free of redshift-space distortions correlation function, taking into account the above statistical correction and under the power-law assumption, is then provided by:

$$\xi(r_p) = \frac{1}{H_\gamma C_\gamma(r_p)} \frac{w_p(r_p)}{r_p}. \quad (26)$$

which can then be fitted to the power-law model (using eq.3) in order to estimate the final and corrected values of the clustering amplitude and slope. Alternatively, one can crudely derive the corrected correlation amplitude (for the slope  $\gamma$  and amplitude  $x_0$  estimated by fitting eq.23) by:

$$x_{0,c} \simeq x_0 C_\gamma(x_0)^{-1/\gamma}, \quad (27)$$

(e.g., Starikova et al. 2011; Koutoulidis et al. 2013). Note that the correction factor values range between  $C_\gamma \simeq 0.85$ , at  $r_p = 3h^{-1}$  Mpc, and  $C_\gamma \simeq 0.45$ , at  $r_p = 10h^{-1}$  Mpc, (for the  $\pi_{\max} = 10h^{-1}$  Mpc case).

### 3.3. Estimating the Angular Correlation Function and Limber's Inversion

Another approach that completely avoids redshift-space distortion effects is to measure the angular correlation function, and then under some assumptions to infer the spatial correlation function through the Limber's inversion equation (Limber 1953).

To this end we estimate the angular correlation function in angular logarithmic bins, covering the range  $10'' < \theta < 3800''$ , for both the complete source sample and the spectroscopic subsample. Furthermore, we numerically estimated the amplitude of

the integral constraint correction (Roche & Eales 1999) which however was found to be negligible, and thus we neglect it in what follows.

It has been demonstrated (Limber 1953) that the angular correlation function,  $w(\theta)$ , can be deprojected to yield the spatial one,  $\xi(r)$ , via an integral equation. Under the power law representation of  $\xi(r)$  (eq.4) the angular correlation length,  $\theta_0$ , is related to the corresponding spatial one,  $x_0$ , at  $z = 0$  according to (Peebles 1980):

$$\theta_0^{\gamma-1} = H_\gamma x_0^\gamma \int_0^\infty \left(\frac{1}{N} \frac{dN}{dz}\right)^2 \frac{d_A(z)^{1-\gamma}}{cd\tau(z)/dz} \tilde{b}^2(z) \tilde{D}^{2+n}(z) dz, \quad (28)$$

where  $d_A$  is the angular diameter distance,  $\tau(z)$  is the look-back time and  $dN/dz$  is the number of sources per unit redshift interval within a solid angle  $\omega_s$  given by:

$$\frac{dN}{dz} = \omega_s d_A(z)^2 (1+z)^2 \phi(z) \left(\frac{c}{H_0}\right) \frac{1}{E(z)} \quad (29)$$

with  $\phi(z) = \int_{L_{\min}(z)}^\infty \Phi(L, z) dL$  the redshift selection function of the sources, i.e., the probability that a source at a comoving distance  $x$  is detected, and  $\Phi(L, z)$  is the luminosity function of the sources<sup>1</sup>.

### 3.4. Construction of the Random Catalogues

In order to create the comparison random sample, mimicking the source catalogue systematic effects and biases, we follow the standard approach, according to which each simulated source is placed at a random position on the part of the sky covered by the survey in hand, with a flux randomly extracted from the observed source  $\log N - \log S$  (Georgakakis et al. 2008). If the flux is above the value allowed by the sensitivity map at that position, the simulated source is kept in the random sample. In the current work we use the AEGIS field sensitivity maps of Laird et al. (2009)

For the spatial correlation function a random redshift is also assigned to each source from the observed source redshift distribution  $N(z)$  (optimally taking into account its variation as a function of flux). As a test of possible disadvantages of this method, caused by the fact that it does not take into account any unknown inhomogeneities and systematics of the follow-up spectroscopic observations, we follow the alternative random catalogue construction approach of Gilli et al. (2005) (hereafter G05). This is based on keeping unaltered the angular coordinates of the sources while reshuffling their redshifts, smoothing the corresponding redshift distribution. For the smoothing we use a Gaussian kernel with a standard deviation of  $\sigma_z = 0.2$ . This offers a compromise between scales that are either too small, and thus may reproduce the  $z$ -space clustering, or too large and thus over-smooth the observed redshift distribution. We verified that our results do not change significantly when using the range:  $\sigma_z = 0.1 - 0.3$ .

## 4. RESULTS

### 4.1. Direct Spatial Correlation Function

In order to estimate the projected correlation function,  $w_p(r_p)$ , we use the estimator provided by eq.(1) and 12 logarithmic separation bins covering the range  $0.5 < r_p < 40h^{-1}$  Mpc. As for

<sup>1</sup> In our case the sources are X-ray selected AGN and the luminosity function that we use is that of the hard-band from (Aird et al. 2010).

**Table 1.** Spatial clustering results for the spectroscopic subsample of the AEGIS field (186 sources within  $0.3 < z < 1.3$ ). The clustering length units are  $h^{-1}$  Mpc. The results correspond to  $\pi_{\max} = 10 h^{-1}$  Mpc. The first row indicates the results based on projected correlation function  $w_p(r_p)$ , while the second corresponds to the corrected spatial correlation function  $\xi(r_p)$  after introducing the correction factor  $C_\gamma(r_p)$  (eq.26). A difference of  $\delta x_0 \simeq +0.9$  is found (for the  $\gamma = 1.8$  case), corresponding to an increase of  $\sim 20\%$  with respect to the uncorrected correlation length value.

	N.of.S	$\gamma$	$x_0$	$x_0 (\gamma = 1.8)$
$w_p(r_p)$	186	$1.7 \pm 0.1$	$4.4 \pm 0.7$	$4.5 \pm 0.7$
$\xi(r_p)$		$1.4 \pm 0.1$	$6.3 \pm 1.5$	$5.4 \pm 1.0$

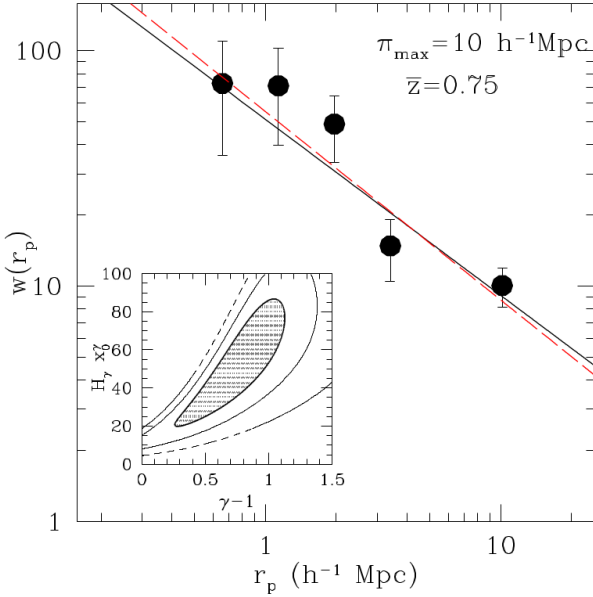


**Fig. 3.** The projected  $w_p(r_p)$  correlation function for the AEGIS field. The black line corresponds to the fit with free  $\gamma$ , while the red line to that for  $\gamma = 1.8$ . The inset panel shows the 1, 2 and  $3\sigma$  likelihood contours in the 2-parameter plane of power law solutions. Note that the y-axis of the inset plot is the combined parameter  $H_\gamma x_0^\gamma$ , since  $H_\gamma$  also depends on the free parameter  $\gamma$  (inspect eq.23).

the choice of  $\pi_{\max}$ , it should be a compromise between having an optimal correlation signal to noise ratio and reducing the excess noise from high  $\pi$  separations, which are affected by redshift-space distortions. We have investigated the sensitivity of  $w_p(r_p)$  on  $\pi_{\max}$ , which we have varied in the range  $[5, 25] h^{-1}$  Mpc; (see also Koutoulidis et al. 2013) and found that it is quite stable. We present the results based on  $\pi_{\max} = 10 h^{-1}$  Mpc.

In Figure 3 we present the derived hard-band projected correlation function. The results of the corresponding power-law fits to the correlation function data are listed in Table 1.

Using the G05 method to construct the random catalogue, we find the best fit correlation length of  $w_p(r_p)$  to be  $x_0 = 4.4 \pm 0.7 h^{-1}$  Mpc (with  $\gamma = 1.7 \pm 0.1$ ), which is in excellent agreement with the total (0.5-8 keV) band result ( $x_0 = 4.3 \pm 0.6 h^{-1}$  Mpc,  $\gamma = 1.6 \pm 0.1$ , reported in Table 2 of Koutoulidis et al. 2013). Once we correct for the factor  $C_\gamma(r_p)$  (eq. 25), the above result translates to a  $\xi(r_p)$  with  $x_{0,c} = 5.4 \pm 1.0 h^{-1}$  Mpc (for  $\gamma = 1.8$ ), which implies that had we not corrected for the intrinsic

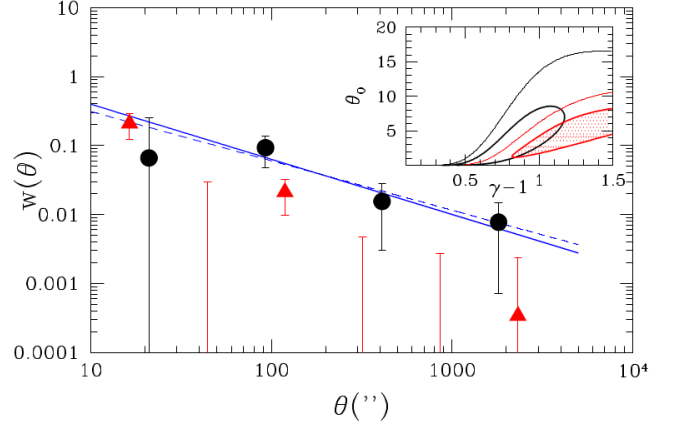


**Fig. 4.** The angular correlation function of the AEGIS field for the subsample with spectroscopic information within  $0.3 < z < 1.3$  (i.e 186 sources, black filled circles) and for the complete X-ray source sample (i.e 741 sources, red filled triangles) in the hard band. The solid line corresponds to the fixed  $\gamma = 1.8$  fit, while the dashed line represents the best power-law fit. The error bars correspond to  $1\sigma$  uncertainties. The inset plot presents the 1 and  $3\sigma$  contours in the fitted  $(\theta_0, \gamma)$  parameter space.

underestimation of  $\xi(r)$  when using the  $w_p(r_p)$  estimator and a finite value of  $\pi_{\max}$  (in our case  $10 h^{-1}$  Mpc), we would have underestimated the true correlation length by  $\sim 20\%$ .

We have also tested and found that these results remain robust when changing the random construction method to that based on the sensitivity map. Our results also agree with other previously derived clustering results of the same field. Coil et al. (2009) derived the AGN/galaxy cross-correlation using 113 Chandra AGN in the full 0.5-7 keV and found  $x_0 = 5.9 \pm 0.9 h^{-1}$  Mpc at a median  $\bar{z} \simeq 0.9$ .

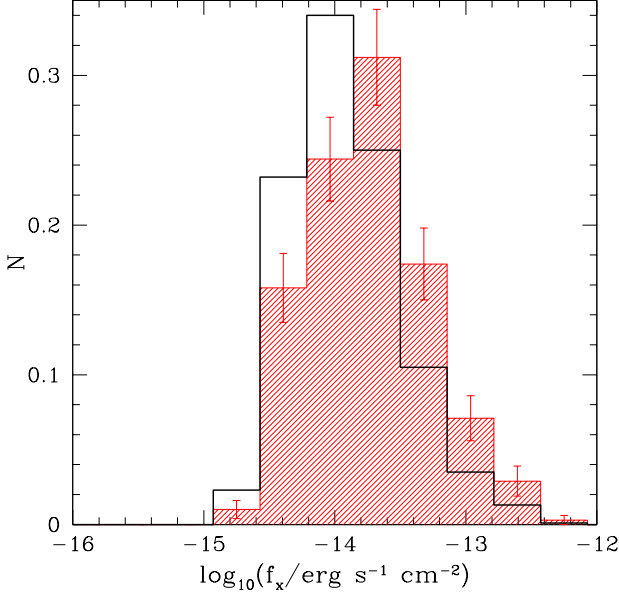
#### 4.2. Angular Correlation function

In Table 2 we present the best fit values of the ACF parameters  $\gamma$  and  $\theta_0$  for the whole and for the spectroscopic subsample, while in Figure 4 we plot the corresponding  $w(\theta)$  for both samples. It is evident that the angular clustering amplitude for the spectroscopic sample (*Spec*) appears significantly larger than that of the whole sample (*All*). We should also point out that the  $w(\theta)$  of the *All* sample has negative values at some separations (as can be inferred from Fig.4), while the power-law fit was performed only on the positive values, a fact which implies that the derived amplitude is an upper limit to the true clustering of this sample. The apparent difference between the ACF of the *Spec* and *All* samples could be attributed to the dependence of clustering on the limiting flux (e.g., Plionis et al. 2008; Ebrero et al. 2009; Elyiv et al. 2012). Indeed, as we show in Figure 5, the flux distributions for the spectroscopic sample (red shaded region) is shifted to higher fluxes with respect to the complete sample of sources (*All*, black thick line), with corresponding mean fluxes are  $f_x \simeq 7.8 \times 10^{-15}$  and  $5.4 \times 10^{-15}$  erg  $s^{-1}$   $cm^{-2}$ , respectively. The observed difference is indeed statistically significant as shown by the Kolmogorov-Smirnov two-sample test which provides a probability of consistency between the two distributions of only  $\sim 2 \times 10^{-8}$ .



**Table 2.** AEGIS hard-band angular correlation function results for the complete sample (*All*) and for those sources with spectroscopic redshifts (*Spec*,  $0.3 < z < 1.3$ ).

	$N$	$\gamma$	$\theta_0''$	$\theta_0'' (\gamma = 1.8)$
<i>All</i>	741	$2.1 \pm 0.2$	$4.3 \pm 1.2$	$1.2 \pm 0.5$
<i>Spec</i>	186	$1.7 \pm 0.1$	$1.6 \pm 1.0$	$2.9 \pm 1.4$

**Fig. 5.** Comparison of the normalized flux distributions of the complete sample (thick black line) and of the spectroscopic subsample (red shaded region).

#### 4.3. Correlation Length by inverting $w(\theta)$

In order to derive the spatial clustering length from the angular correlation function we use eq.(28) and as the source  $N(z)$  distribution we use either the integral of the hard-band Luminosity and Density Evolution (LADE) luminosity function (Aird et al. 2010) or directly the redshift distribution of the sources with available spectroscopic redshifts. Both approaches lead to exactly the same results and thus we present results based on the later approach.

The next step in order to derive the spatial clustering length is to somehow estimate the exponent of the growth factor,  $\bar{D}^{2+n}(z)$ . One could therefore use literature clustering estimates of hard-band AGN samples, dominating different redshifts, and fit eq.(13) to such data. Since however, the available hard-band results are very few; i.e., that of (Mountrichas & Georgakakis 2012) with  $r_0 = 4.8 \pm 1 h^{-1}$  Mpc at  $\bar{z} = 0.1$  and of CDF-N with  $r_0 = 5 \pm 1 h^{-1}$  Mpc at  $\bar{z} = 0.9$  (Gilli et al. 2005)<sup>2</sup>, we will also use total band (0.5-8 keV) clustering results (e.g., Coil et al. 2009; Starikova et al. 2011; Allevato et al. 2011; Koutoulidis et al. 2013) excluding the results of  $\bar{z} \approx 0.75$  which appears to present an erratic behaviour in all available studies (see Fig.8 and relevant discussion in Koutoulidis et al. 2013). It appears that there is a weak but consistent increase of the value of  $x_0$  with redshift. The use of total band results is also supported by the fact that the corresponding AEGIS correlation function results are in excellent agreement with those of the hard-band, as discussed previously.

<sup>2</sup> The correlation length of CDF-S ( $r_0 = 9.8 \pm 1 h^{-1}$  Mpc at  $\bar{z} = 0.7$ ) is not considered due to the presence of superclusters which affect the clustering amplitude (Gilli et al. 2003).

**Table 3.** Comparison of the inverted ACF AEGIS hard-band correlation length,  $x_0$  (in  $h^{-1}$  Mpc), and that directly measured by at  $\bar{z} = 0.1$  (Mountrichas et al. 2012) and  $\bar{z} = 0.75$  (our current measure).

$\bar{z}$	$w(\theta)$ based	$\xi(r_p)$ based
0.10	$5.0 \pm 1.1$	$4.8 \pm 1.0$
0.75	$5.5 \pm 1.2$	$5.4 \pm 1.0$

Subsequently, we perform a  $\chi^2$  minimisation fitting of the above data to eq. (13), leaving as a free parameter the exponent  $n$  and fixing the halo mass to  $M_h = 1.3 \times 10^{13} M_\odot$ , which we derived in Koutoulidis et al. (2013). The resulting best fit value for the exponent is  $2 + n = 5.03 \pm 0.2$ . The corresponding  $\chi^2 - \chi^2_{min}$  and clustering evolution curves can be seen in the left and right panels of Figure 6, respectively (in black). Alternatively we can leave as free parameters both the exponent  $n$  and the halo mass  $M_h$ . In this case the minimization procedure provides a degenerate solution, similar to that of Fig.2. As an example, we present in the right panel of Figure 6 another clustering evolution model (red curve), that with  $(n, M_h) \approx (2.0, 2 \times 10^{12} M_\odot)$ , consistent with the data and selected from within the  $1\sigma$  range of the degenerate solution.

Taking into account the above parameters and using eq.(28) we deproject the ACF and derive the spatial clustering length. Since the Limber's inversion provides the spatial clustering length at  $z = 0$ , in order to predict its value at another redshift it is necessary to normalized eq.(13) to that redshift. As seen in Table 3, normalizing to  $z = 0.75$ , which corresponds to the median redshift of the spectroscopic AEGIS hard-band sample, we find an excellent agreement between the direct measure of  $x_0$  and the corresponding Limber's inverted one. Similarly, normalizing to  $z = 0.1$  which is the median redshift of the sample studied in (Mountrichas & Georgakakis 2012) we again find an excellent agreement with the direct  $x_0$  measure (see Table 3).

Since the parameterisation of X-ray AGN clustering evolution (eq.10) reproduces the direct spatial correlation length for a particular value of  $n$ , we apply it also to the clustering results of the whole AEGIS X-ray source sample ( $\theta_0 = 1.2 \pm 0.6$  arcsec with  $\gamma = 1.8$  - Table 2). We use the expected  $N(z)$ , based on the LADE luminosity function of Aird et al. (2010), but for the whole interval  $z = 0 - 4$ , since we cannot a priori assess if the sources without redshifts correspond to nearby low-luminosity or distant high-luminosity sources. The predicted median redshift of this sample is  $\bar{z} = 0.98$ . Using Limber's inversion we obtain  $r_0 = 4.8 \pm 0.9 h^{-1}$  Mpc at  $z = 0.1$  and  $r_0 = 5.5 \pm 1.0 h^{-1}$  Mpc at  $z = 0.1$  and  $z = 0.75$ , respectively, which are in excellent agreement with the scaled  $0.3 < z < 1.3$  and the direct  $\xi(r_p)$  results (see Table 3). Given these results we can infer that the sources without redshift information seem to follow roughly the same clustering evolution as the observed. Moreover the above procedure indicates the potential for an accurate derivation of the spatial correlation length using only the angular clustering of all the available sources, independently of availability or not of complete spectral information, for as long as the luminosity function in hand relates to the whole sample of sources.

## 5. DISCUSSION & CONCLUSIONS

A variety of studies have measured the projected angular clustering of X-ray AGN, and then via Limber's equation derived the corresponding spatial clustering length. Although there are obvious merits in this approach, i.e., the fact that one uses all the

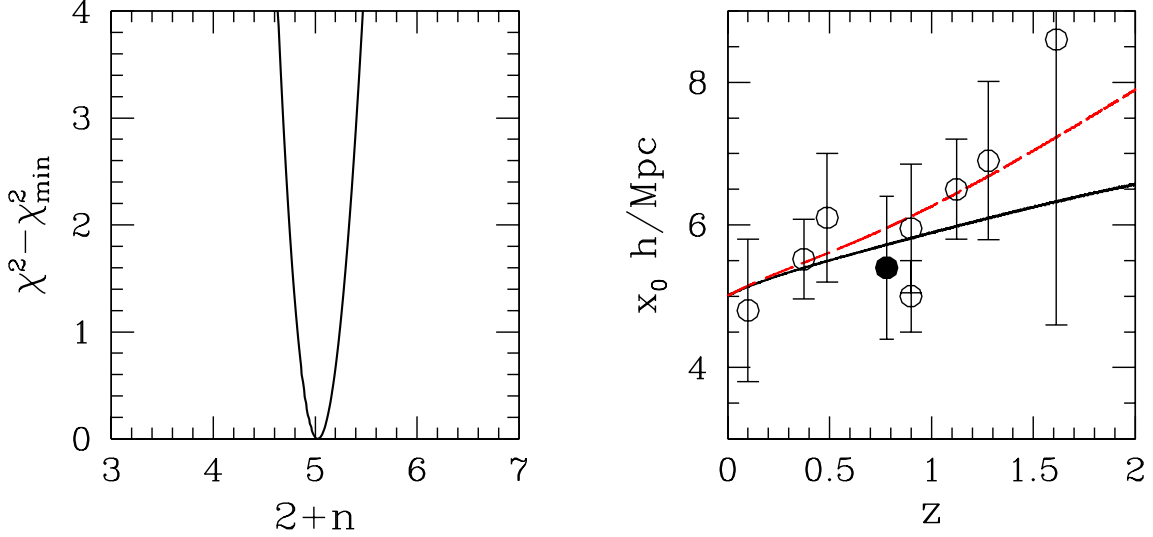


**Fig. 6.** *Left panel:* Result of the  $\chi^2$  minimisation procedure of fitting the parameter  $2 + n$ . *Right panel:* The clustering evolution model (black curve), corresponding to the best fit value ( $n = 3.03$ ) for  $M_h = 1.3 \times 10^{13} M_\odot$ , overplotting the literature  $x_0$  data in the hard and total band. Our direct estimate (not used in the  $\chi^2$  minimization procedure) is shown as the filled circle. As a manifestation of the degeneracy discussed in section 2, we show the expected clustering evolution for another ( $n, M_n$ ) pair  $\approx (2.0, 2 \times 10^{12} M_\odot)$  which is consistent with the data (red curve).

available sources while being unaffected by redshift-space distortions, there are disadvantages and inherent assumptions in the deprojection the most important of which is the unknown clustering evolution model of the sources. There have been interesting parametrizations of such an evolution, the most common of which is the  $1 + z$  power law model (the so-called  $\epsilon$  models; see Eq.5), which has been used extensively to model the evolution of clustering. However, it is rather phenomenological in nature and thus it does not provide a good physical insight into the evolution governed by the clustering of dark matter halos (McCracken et al. 2001). In this work we presented a more generic parametrization that allows for different cosmological models and different host dark matter halo mass, via their different bias evolution, and we showed the regimes where the two parametrizations coincide.

One can identify two interesting extremes of the clustering evolution; The stable clustering scenario ( $\epsilon = 0$  or  $n \gtrsim 4.2$  depending also on the halo mass, for the two different parametrizations, respectively) in which clusters remain bound and stable while due to the expansion the background density drops by  $(1 + z)^3$  and the constant in comoving coordinates scenario ( $\epsilon = \gamma - 3$  or  $n \lesssim 3.5$ ; see section 2) in which pairs of sources follow the Hubble flow, meaning that their separation remains constant in comoving coordinates. Interestingly, the correlation function analyses of optically selected QSO samples (Croom et al. 2005; Ross et al. 2009) seem to suggest a roughly comoving evolution model of their clustering, while simulations also seem to disfavour the stable clustering evolution model (Jain 1997).

In this work, we used the comoving clustering lengths of X-ray AGN at a variety of different redshifts, provided in the literature (Gilli et al. 2005; Coil et al. 2009; Starikova et al. 2011; Allevato et al. 2011; Mountrichas & Georgakakis 2012; Koutoulidis et al. 2013), to fit the unknown slope of the non-

linear contribution to the growing mode of perturbations in order to model the evolution of clustering of X-ray AGN. We then applied this to the Limber's inversion of the angular correlation function of the subsample of AEGIS X-ray AGN with spectroscopic data within  $0.3 < z < 1.3$  to find an excellent agreement with the directly measured spatial clustering of the same sources.

The reason of the discrepancies between angular and spatial clustering results of various previous studies is still not clearly identified, although the clustering evolution parametrization, used in this work, does hint towards the possibility that the different host halo mass for the different sources, and thus their different bias evolution, induce a different clustering evolution than what one assumes when using the phenomenological  $\epsilon$  parametrization.

The present work appears to pave the way for the application of the angular correlation function analysis on large X-ray selected AGN samples, such as the eROSITA survey which is expected to detect over  $3 \times 10^6$  AGN. Such numbers of sources render rather impossible the use of spectroscopic redshifts to derive their spatial clustering, as this would demand unrealistically large follow-up optical telescope time.

## References

- Aird, J., Nandra, K., Laird, E. S., et al. 2010, MNRAS, 401, 2531
- Akylas, A., Georgantopoulos, I., & Plionis, M. 2000, MNRAS, 318, 1036
- Alexander, D. M. & Hickox, R. C. 2012, Nar, 56, 93
- Allevato, V., Finoguenov, A., Cappelluti, N., et al. 2011, ApJ, 736, 99
- Barger, A. J. 2005, Royal Society of London Philosophical Transactions Series A, 363, 685
- Basilakos, S., Dent, J. B., Dutta, S., Perivolaropoulos, L., & Plionis, M. 2012, PRD, 85, 123501
- Basilakos, S., Georgakakis, A., Plionis, M., & Georgantopoulos, I. 2004, ApJ, 607, L79
- Basilakos, S. & Plionis, M. 2001, ApJ, 550, 522
- Basilakos, S. & Plionis, M. 2003, ApJ, 593, L61



- Basilakos, S., Plionis, M., Georgakakis, A., & Georgantopoulos, I. 2005, *MNRAS*, 356, 183
- Basilakos, S., Plionis, M., & Pouri, A. 2011, *PRD*, 83, 123525
- Basilakos, S., Plionis, M., & Ragone-Figueroa, C. 2008, *ApJ*, 678, 627
- Bournaud, F., Dekel, A., Teyssier, R., et al. 2011, *ApJ*, 741, L33
- Cappelluti, N., Ajello, M., Burlon, D., et al. 2010, *ApJ*, 716, L209
- Coil, A. L., Georgakakis, A., Newman, J. A., et al. 2009, *ApJ*, 701, 1484
- Croom, S. M., Boyle, B. J., Shanks, T., et al. 2005, *MNRAS*, 356, 415
- Davis, M., Faber, S. M., Newman, J., et al. 2003, in *Society of Photo-Optical Instrumentation Engineers (SPIE) Conference Series*, Vol. 4834, *Society of Photo-Optical Instrumentation Engineers (SPIE) Conference Series*, ed. P. Guhathakurta, 161–172
- Davis, M., Newman, J. A., Faber, S. M., & Phillips, A. C. 2001, in *Deep Fields*, ed. S. Cristiani, A. Renzini, & R. E. Williams, 241
- Davis, M. & Peebles, P. J. E. 1983, *ApJ*, 267, 465
- de Zotti, G., Persic, M., Franceschini, A., et al. 1990, *ApJ*, 351, 22
- Di Matteo, T., Springel, V., & Hernquist, L. 2005, in *Growing Black Holes: Accretion in a Cosmological Context*, ed. A. Merloni, S. Nayakshin, & R. A. Sunyaev, 340–345
- Ebrero, J., Mateos, S., Stewart, G. C., Carrera, F. J., & Watson, M. G. 2009, *A&A*, 500, 749
- Elyiv, A., Clerc, N., Plionis, M., et al. 2012, *AAP*, 537, A131
- Fanidakis, N., Baugh, C. M., Benson, A. J., et al. 2012, *MNRAS*, 419, 2797
- Fanidakis, N., Georgakakis, A., Mountrichas, G., et al. 2013, *MNRAS*, 435, 679
- Fry, J. N. 1996, *ApJ*, 461, L65
- Georgakakis, A., Nandra, K., Laird, E. S., Aird, J., & Trichas, M. 2008, *MNRAS*, 388, 1205
- Gilli, R., Cimatti, A., Daddi, E., et al. 2003, *ApJ*, 592, 721
- Gilli, R., Daddi, E., Zamorani, G., et al. 2005, *A&A*, 430, 811
- Gilli, R., Zamorani, G., Miyaji, T., et al. 2009, *A&A*, 494, 33
- Groth, E. J. & Peebles, P. J. E. 1977, *ApJ*, 217, 385
- Hamilton, A. J. S. 1993, *ApJ*, 417, 19
- Hickox, R. C., Jones, C., Forman, W. R., et al. 2009, *ApJ*, 696, 891
- Hopkins, P. F. & Hernquist, L. 2006, *ApJS*, 166, 1
- Hopkins, P. F., Hernquist, L., Cox, T. J., et al. 2006, *ApJ*, 163, 1
- Jain, B. 1997, *MNRAS*, 287, 687
- Koutoulidis, L., Plionis, M., Georgantopoulos, I., & Fanidakis, N. 2013, *MNRAS*, 428, 1382
- Krumpe, M., Miyaji, T., & Coil, A. L. 2010, *ApJ*, 713, 558
- Laird, E. S., Nandra, K., Georgakakis, A., et al. 2009, *ApJ*, 180, 102
- Li, C., Kauffmann, G., Wang, L., et al. 2006, *MNRAS*, 373, 457
- Limber, D. N. 1953, *ApJ*, 117, 134
- McCracken, H. J., Le Fèvre, O., Brodwin, M., et al. 2001, *AAP*, 376, 756
- Miyaji, T., Zamorani, G., Cappelluti, N., et al. 2007, *ApJ*, 172, 396
- Mo, H. J., Jing, Y. P., & Boerner, G. 1992, *ApJ*, 392, 452
- Mountrichas, G. & Georgakakis, A. 2012, *MNRAS*, 420, 514
- Mountrichas, G., Georgakakis, A., Finoguenov, A., et al. 2013, *MNRAS*, 430, 661
- Mullis, C. R., Henry, J. P., Gioia, I. M., et al. 2004, *ApJ*, 617, 192
- Papageorgiou, A., Plionis, M., Basilakos, S., & Ragone-Figueroa, C. 2012, *MNRAS*, 422, 106
- Peebles, P. J. E. 1980, *The large-scale structure of the universe*
- Peebles, P. J. E. 1993, *Principles of Physical Cosmology*
- Plionis, M., Rovilos, M., Basilakos, S., Georgantopoulos, I., & Bauer, F. 2008, *ApJ*, 674, L5
- Porciani, C. & Norberg, P. 2006, *MNRAS*, 371, 1824
- Puccetti, S., Fiore, F., D’Elia, V., et al. 2006, *AAP*, 457, 501
- Roche, N. & Eales, S. A. 1999, *MNRAS*, 307, 703
- Ross, N. P., Shen, Y., Strauss, M. A., et al. 2009, *ApJ*, 697, 1634
- Shen, Y., Strauss, M. A., Ross, N. P., et al. 2009, *ApJ*, 697, 1656
- Sheth, R. K. & Tormen, G. 1999, *MNRAS*, 308, 119
- Starikova, S., Cool, R., Eisenstein, D., et al. 2011, *ApJ*, 741, 15
- Tinker, J. L., Robertson, B. E., Kravtsov, A. V., et al. 2010, *ApJ*, 724, 878
- Vikhlinin, A. & Forman, W. 1995, *ApJ*, 455, L109
- Wolf, C., Wisotzki, L., Borch, A., et al. 2003, *AAP*, 408, 499
- Xue, Y. Q., Luo, B., Brandt, W. N., et al. 2011, *APJS*, 195, 10
- Yang, Y., Mushotzky, R. F., Barger, A. J., & Cowie, L. L. 2006, *ApJ*, 645, 68